Journal of Power Sources 246 (2014) 736–746

Contents lists available at ScienceDirect

Journal of Power Sources

journal homepage: www.elsevier.com/locate/jpowsour

Modeling and energy management control design for a fuel cell hybrid passenger bus

Kyle Simmons [a,b,*], Yann Guezennec [a,b], Simona Onori [a]

[a] Center for Automotive Research, The Ohio State University, Columbus, OH 43212, USA
[b] Mechanical and Aerospace Engineering Department, The Ohio State University, Columbus, OH 43212, USA

HIGHLIGHTS

- Development of an energy-based simulator for a fuel cell/battery hybrid passenger bus.
- Experimental identification of equivalent circuit model for a lithium ion iron phosphate battery.
- Optimal control implementation for supervisory energy management using Pontryagin's Minimum Principle.
- Design and tuning of a practical controller tuned against the optimal solution.
- Comparative analysis of ARMA and PMP controllers.

ARTICLE INFO

Article history:
Received 2 June 2013
Received in revised form
25 July 2013
Accepted 5 August 2013
Available online 15 August 2013

Keywords:
Fuel cell
Hybrid vehicles
Li-ion batteries
Modeling
Control

ABSTRACT

This paper presents the modeling and supervisory energy management design of a hybrid fuel cell/battery-powered passenger bus. With growing concerns about petroleum usage and greenhouse gas emissions in the transportation sector, finding alternative methods for vehicle propulsion is necessary. Proton Exchange Membrane (PEM) fuel cell systems are viable possibilities for energy converters due to their high efficiencies and zero emissions. It has been shown that the benefits of PEM fuel cell systems can be greatly improved through hybridization. In this work, the challenge of developing an on-board energy management strategy with near-optimal performance is addressed by a two-step process. First, an optimal control based on Pontryagin's Minimum Principle (PMP) is implemented to find the global optimal solution which minimizes fuel consumption, for different drive cycles, with and without grade. The optimal solutions are analyzed in order to aid in development of a practical controller suitable for on-board implementation, in the form of an Auto-Regressive Moving Average (ARMA) regulator. Simulation results show that the ARMA controller is capable of achieving fuel economy within 3% of the PMP controller while being able to limit the transient demand on the fuel cell system.

1. Introduction

The transportation sector accounted for approximately 26% of the world's overall energy consumption in 2012, with 94% of that energy being produced by burning petroleum [1]. Burning fossil fuels releases numerous greenhouse gas emissions that can adversely affect the environment. It is estimated that the transportation sector contributes around 20% of the world's total greenhouse gas emissions [2]. Governments and private companies alike are committed to find alternative methods for energy generation in an effort to reduce fossil fuel usage and greenhouse gas emissions, and to create safe, sustainable energy.

These factors have led to tremendous amounts of research being conducted to increase fuel economy in today's vehicles. Different ways to improve the efficiency of conventional vehicle propulsion systems as well as exploring advanced propulsion systems, such as electric vehicles, hybrid electric vehicles (HEV), hydraulic hybrid vehicles, and fuel cell vehicles have been proposed. This paper focuses on modeling, simulation and supervisory control design for a hybrid fuel cell passenger bus.

Proton Exchange Membrane (PEM) fuel cells are an attractive alternative energy conversion device for automotive propulsion. As electrochemical devices, fuel cells convert chemical energy into electrical energy directly without mechanical processes. PEM fuel cells are favorable for their zero emissions, relatively high

* Corresponding author. Center for Automotive Research, The Ohio State University, Columbus, OH 43212, USA. Tel.: +1 330 466 6335.
E-mail address: simmons.429@osu.edu (K. Simmons).

0378-7753/$ – see front matter © 2013 Elsevier B.V. All rights reserved.
http://dx.doi.org/10.1016/j.jpowsour.2013.08.019

efficiency, and low noise generation [3]. Advances in the past 10–15 years have significantly increased their power density and ability to follow dynamic loads, making them viable for automotive applications. However, their high cost and relatively shorter life than internal combustion engines make commercialization difficult. Further development of the fuel cell technology and their integration into vehicles is needed for significant market penetration to be possible. To help increase the rate of commercialization, the Federal Transit Authority (FTA) created the National Fuel Cell Bus Program (NFCBP) in 2006. The overall goal of the program is to assist in development and demonstration of fuel cell technology for transit buses, and to improve commercial viability [4]. Through the program, the FTA hopes to achieve the following:

- facilitate the development of fuel cell technology, primarily for full-size, heavy duty transit bus applications;
- improve transit bus efficiency, reduce petroleum consumption, and reduce emissions;
- improve fuel cell durability, reliability, and reduce overall fuel cell bus cost;
- establish a globally competitive U.S. industry for fuel cell bus technology;
- increase public awareness and acceptance of fuel cell vehicles.

The FTA has committed nearly $90 million to the NFCBP, with an equal amount coming from private companies. This has funded the development of 25 fuel cell bus demonstrations that are currently in operation, with 7 more demonstrations under development. These projects are all competitively selected by the FTA and are located across the country.

The work presented in this paper has been funded under one of these projects. The Center for Automotive Research (CAR) at The Ohio State University (OSU) was invited to act as a sub-contractor to the DesignLine Corporation [5] through an ongoing award from the NFCBP through the Center for Transportation and the Environment by aiding in the development of an energy-based model of a hybrid fuel cell bus proposed and developed by DesignLine and to assist in the design of the supervisory energy management of the bus.

The paper is structured as follows: in Section 2, a brief introduction to the energy management control problem in hybrid vehicles is given, with a focus on strategies proposed for hybrid fuel cell vehicles. Section 3 presents the powertrain architecture of the selected bus and the energy-based vehicle simulator. In Section 4, the optimal control problem for the energy management of the hybrid fuel cell bus is formulated which aims to minimize the mass of hydrogen used on-board while guaranteeing a safe operation of the battery. The optimal energy management problem is then solved by means of PMP [6] which provides a proxy for a global optimal solution. Achieved fuel economy, battery operation, and fuel cell operation are examined over different driving scenarios with and without grades in Section 5. The analysis conducted leads to the development of a practical controller which is suitable for on-board implementation. A comparison of the performance of both strategies is presented. In Section 7 conclusions and final remarks are discussed.

2. Hybrid vehicle energy management

The extra degree of freedom offered by the hybrid topology introduces the need for an energy management control strategy [7]. The fuel cell hybrid bus needs an Energy Management Strategy (EMS) to distribute electrical power among the load and distinct power sources. The strategy must satisfy powertrain component constraints while trying to achieve some system-level performance objective such as maximizing fuel economy, maintaining the battery state-of-charge (SOC), or improving the life of the components. Numerous are the contributions from the literature on control techniques for HEVs, many of which have been extended to a fuel cell hybrid vehicle [8–10]. In general, the design methods for EMS reported in literature can be categorized into:

- Rule-based approaches
- Optimization approaches

Rule-based strategies can be easily implementable for real-time application and are usually based on heuristics [11]. Performance of these strategies can be improved through the use of fuzzy logic or adaptively altering rules during a driving event [12–17]. Among the optimization approaches there are global and instantaneous strategies. One such instantaneous optimization technique is the equivalent consumption minimization strategy (ECMS) [18]. Paganelli [19] and Rodatz et al. [20] presented an ECMS for fuel cell vehicles in which the cost function was evaluated based on hydrogen consumption and the equivalent fuel consumption for the energy storage system. An equivalent fuel consumption for on-board energy sources that do not use a conventional fuel (i.e. batteries, super capacitors) has been defined. The cost function that is minimized can be fuel consumption [21] or emissions [22].

Another instantaneous optimization strategy is based on Pontryagin's Minimum Principle [23]. PMP introduces a co-state variable which when properly tuned provides the optimal solution for a given drive cycle. In Ref. [24], PMP is used to find the globally optimal solution for a fuel cell vehicle, which can only be done off-line. In order to implement the strategy in real time, the authors adaptively change the value of the co-state during a drive cycle to ensure charge sustainability of the battery.

Feroldi et al. [25] developed three energy management strategies, based on the efficiency curve of the fuel cell system, for electric vehicles powered by hybrid power systems. One of the strategies was attained by utilizing a constrained non-linear programming method. Other strategies were attained by analysis on empirical observations. Delprat and Bernard [26,27] matured the EMS by forward iteration of a state equation, a co-state equation, and a stationary equation with an assumption that the initial co-state vector was available. This approach is a non-casual solution because knowledge of the driving cycle must be available for off-line optimization.

Global optimization strategies, such as dynamic programming (DP) [28], minimize a performance metric for a specified drive cycle, which must be known *a priori*. DP has been used in Ref. [29] to find the minimal cost of operating a fuel cell bus. It has been shown in Ref. [30] that through proper tuning of instantaneous minimization strategies, the optimal solution can be found for a given drive cycle. These optimal solutions are often used as a benchmark for comparison when testing a real-time control strategy. However, these solutions are also used as a basis for designing implementable strategies. As was done in Ref. [31], a rule-based strategy can be designed by first finding the global optimal solution given by DP and then deriving rules from observing the optimal behavior.

In this paper a similar approach is taken. The optimal solution to the control problem is found for multiple drive cycles, with and without grade, using PMP. A practical controller is then developed and tuned based on the observations and analysis of the optimal behavior. Design and tuning of the practical controller was done to mimic the optimal results and obtain sub-optimal fuel consumption results. To the best of knowledge of the authors, this is a novel approach which has not yet been presented in the literature.

3. Parallel hybrid fuel cell bus simulator

The powertrain architecture of the hybrid fuel cell bus is a parallel hybrid, battery dominated powertrain with a fuel cell system functioning primarily as an auxiliary power unit. The battery and fuel cell supply electrical power directly to the bus's two rear-wheel electric traction motors as well as to the auxiliary loads (HVAC, lighting, integrated fuel cell compressor, etc.). A schematic of the powertrain components specified by DesignLine is shown in Fig. 1

The component specifications are shown in Table 1.

3.1. Hybrid Powertrain modeling

A forward-looking, energy-based simulator [32] was built to simulate the bus behavior, analyze the on-board energy flow, and develop energy management strategies. The forward simulator, whose structure is shown in Fig. 2, consists of the following functional blocks:

- Driving Profile;
- Driver;
- Supervisory Controller;
- Hybrid Powertrain;
- Vehicle Dynamics.

The *Driving Profile* module contains a desired velocity profile, $v_{cyc}(t)$, that can be either a standard cycle or experimentally obtained. When applicable, a corresponding road grade profile is also issued together with the desired velocity profile. The *Driver* is implemented as a PID controller [32] that based on the difference between the desired velocity and the current velocity of the simulated vehicle, $v_{veh}(t)$, provides an acceleration or deceleration command at each time step. These commands are converted to a mechanical power demand for the powertrain, $P_{EM,m}(t)$. Once converted to an electrical power (through the EM efficiency) and added to the bus's auxiliary loads, P_{aux}, the total power request, P_{req}, is given by:

$$P_{req}(t) = P_{EM,e}(t) + P_{aux}(t) \quad (1)$$

The total auxiliary, P_{aux}, load consists of the two terms: $P_{aux,\,elec}$ which accounts for all of the electrical accessories on the bus, and $P_{aux,FC}$ which accounts for the integrated fuel cell system compressor. Both of these will be discussed later. P_{aux} is found by:

$$P_{aux}(t) = P_{aux,elec}(t) + P_{aux,FC}(t) \quad (2)$$

The total power request can be satisfied using the fuel cell and the battery to supply electrical power to the electric motors and auxiliary loads:

Table 1
Powertrain components sizing.

Fuel cell system	Ballard FC*velocity*-HD6, 75 kW max power
Battery	GAIA Lithium Ion Iron Phosphate Cells (LFP), 38 Ah/3.2 V/122 Wh, $180S \times 2P$ pack, 45 kWh pack size
Electric Motors (EM)	2 ZF motors, 21,000 Nm max torque, 1150 rad s^{-1} max speed, constant 22.63 gear ratio
Power Electronics	Acceptable Voltage range: [480,692] V

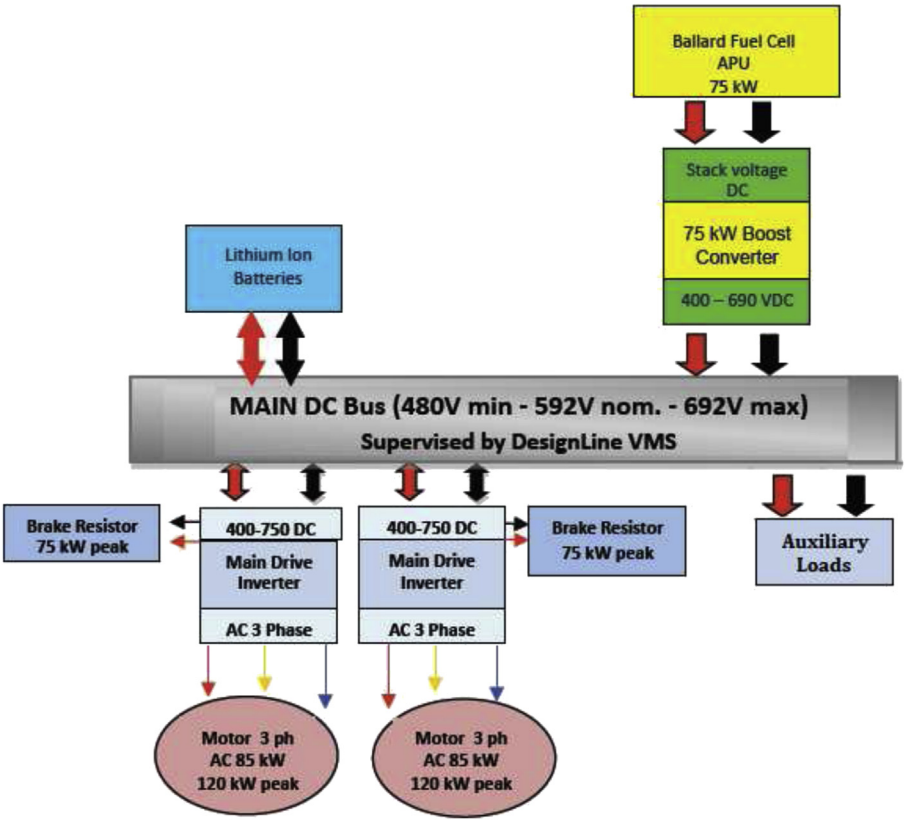

Fig. 1. Proposed bus powertrain.

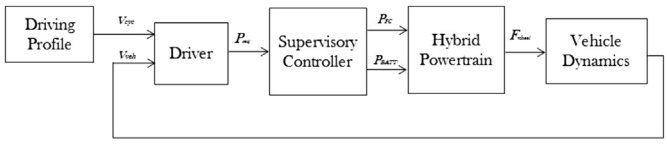

Fig. 2. Schematic of the forward-looking vehicle simulator.

$$P_{FC}(t) + P_{batt}(t) = P_{req}(t) \tag{3}$$

where P_{FC} is the power supplied by the fuel cell stack and P_{batt} is the power supplied by the battery. Fig. 3 shows the power flow through the powertrain. The *Supervisory Controller*, which determines the actuator set points, P_{FC} and P_{batt},[1] to be sent to the Hybrid Powertrain Module, is described in Section 4. Its design is the main topic of this paper.

The fuel cell and battery power sent to the electric motors (by means of Eqs. (1) and (3)) is converted into a tractive force at the wheel. Through the longitudinal dynamics of the bus, the vehicle velocity can be calculated using:

$$m\frac{dv_{veh}}{dt} = F_{wheel} - F_r - F_a - F_g \tag{4}$$

where m is the mass of the bus, dv_{veh}/dt is the longitudinal acceleration of the bus, F_{wheel} is the force at the wheel supplied by the powertrain, and F_r, F_a, and F_g are the rolling resistance, aerodynamic drag, and grade forces respectively. These are calculated by:

$$F_r = m\cdot g\cdot\cos\theta\cdot c_r\cdot v_{veh} \tag{5}$$

$$F_a = \frac{1}{2}\cdot_{air}\cdot c_d\cdot A_f\cdot v_{veh}^2 \tag{6}$$

$$F_g = m\cdot g\cdot\sin\theta \tag{7}$$

where θ [rad] is the road grade angle, c_r is the rolling resistance coefficient, ρ_{air} is the density of air, c_d is the aerodynamic drag coefficient, and A_f is the frontal area of the bus.

Integration of Eq. (4) with respect to time provides the velocity of the vehicle, v_{veh}, which is fed back to the driver for comparison with the desired drive cycle. Table 2 provides the values of the vehicle parameters used in the simulator (Fig. 3).

3.2. Powertrain components

3.2.1. Fuel cell stack

The Ballard fuel cell stack used in this study is depicted in Fig. 4 [33]. The model for the fuel cell used in this simulator is a static model which neglects dynamic behavior. This is adequate for the purpose of vehicle energy analysis and fuel consumption estimation. The power output of the fuel cell model, while dependent on temperature, air pressure and humidification of the fuel cell, is set by the manufacturer's controller to adequately maintain these in accordance with the fuel cell operating point. These effects are incorporated with the data provided by Ballard, yielding a net system characteristic curve.

The experimental data obtained from Ballard provided a power-to-current relationship of the fuel cell. Fig. 5 shows the sparse experimental data as well as the 2nd order polynomial curve-fit used for the model. It is important to note that in reality Ballard prevents the fuel cell from operating below an output power of 5 kW in order to maintain safe operation and functionality of the system.

The curve-fit is defined by:

$$I_{FC} = 0.0041\cdot P_{FC}^2 + 2.8411\cdot P_{FC} - 0.3913 \tag{8}$$

where I_{FC} [A] is the required current to produce a stack power output of P_{FC} [kW]. This equation is only valid for $5 \le P_{FC} \le 75$. Knowing the electric current required to produce a given amount of power also allows for hydrogen mass flow rate estimation. The hydrogen mass flow rate of the fuel cell is given as an increasing linear relationship to the electrical current level, I_{FC} which was experimentally obtained by the manufacturer to be equal to:

$$\dot{m}_H = 0.00435\cdot I_{FC} \tag{9}$$

where $\dot{m}_H$ [kg s^{-1}] is the mass flow rate of hydrogen.

3.2.2. Fuel cell compressor

A compressor is a sub-component of the fuel cell system. It is needed to pressurize the air supply to the fuel cell stack for proper functioning and optimal operation. While commanded by the fuel cell system controller, it is externally powered, hence this affects the overall efficiency of the fuel cell system. From experimental data from the manufacture for the specific compressor selected for the fuel cell system, a static model was developed. The relationship between the operating current of the fuel cell and the electrical power consumption of the motor driving the compressor is given as:

$$P_{aux,FC} = 0.000082\cdot I_{FC}^2 + 0.0092\cdot I_{FC} + 0.4885 \tag{10}$$

where $P_{aux,FC}$ [kW] is the power consumption of the compressor at a fuel cell operating current, I_{FC}. This power consumption by the compressor is added to the total auxiliary power demand by the bus by Eq. (2).

3.2.3. DC/DC converter

Because the output voltage of the fuel cell system is not within the acceptable voltage range of other powertrain components on

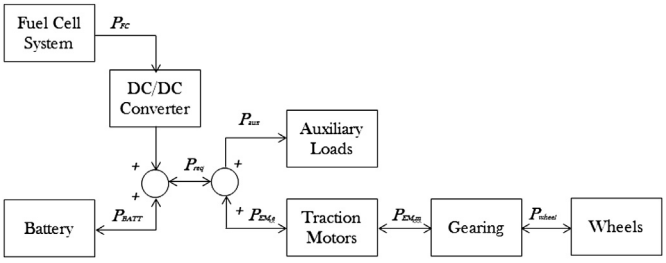

Fig. 3. Power flow through Powertrain.

Table 2
Vehicle dynamics parameters.

Parameter	Parameter description	Value used in simulator
m	Vehicle mass	15875.7 kg
g	Gravitational acceleration	9.81 m s^{-2}
c_r	Rolling resistance coefficient	.006
ρ_{air}	Density of air	1.29 kg m
c_d	Aerodynamic drag coefficient	0.54
A_f	Frontal surface area of bus	7.5 m^2

[1] By convention, positive power corresponds to discharging the battery, negative power corresponds to charging.

Fig. 4. Ballard HD6 75 kW Fuel Cell.

the bus, a DC/DC converter is needed. This ensures voltage supplied to other electrical systems on the bus is within the acceptable range. The DC/DC converter is modeled in a very simplified fashion as an affine function having a constant efficiency with a constant power loss term:

$$\overline{P_{FC}} = P_{FC} \cdot \eta_{DC} - P_{loss} \tag{11}$$

where $\overline{P_{FC}}$ is the output power, P_{FC} is the input power, η_{DC} is the efficiency, and P_{loss} is a constant power loss of the DC/DC converter. Table 3 shows the parameter values used in the simulator.

3.2.4. Battery

An accurate dynamic model of the battery system is essential for determination of battery SOC. Through experimental observations, it has been found that the current-to-voltage behavior of batteries used in hybrid vehicle platforms display significant dynamical behavior which are linked to electrochemistry, ion diffusion etc. [34,35]. These factors are very complex and difficult to predict by first principle models, however it has been shown that the net electrical dynamical behavior can be well predicted through approximation by an equivalent electrical circuit of reduced order [36].

A 2nd order equivalent electrical circuit model of a battery, used in this work, is shown in Fig. 6. As the order of the circuit, hence the number of RC pairs increases, so does the accuracy of the model. The number of unknown parameters also increases.

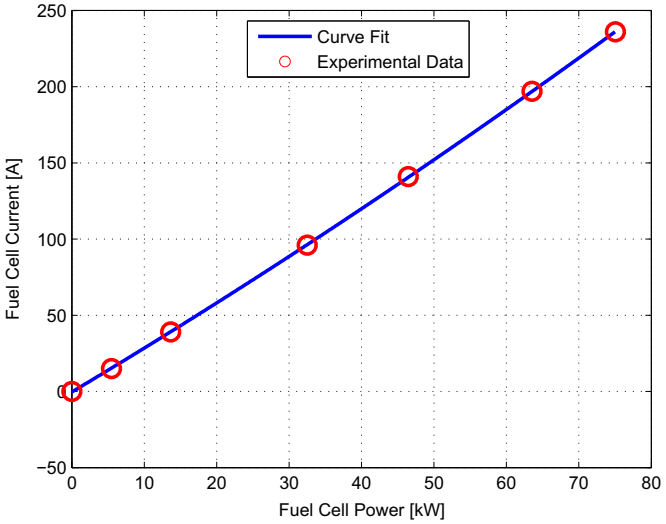

Fig. 5. Fuel cell stack current–power relationship.

Table 3
DC/DC converter parameters.

Parameter	Value used in simulator
η_{DC}	0.98
P_{loss}	1 kW

The circuit consists of an ideal voltage source or open circuit voltage, V_{OC}, an internal resistance, R_0, two RC pairs, and a hysteresis voltage, V_h. V_{Ci} is the voltage across the ith capacitor ($i = 1,2$), R_i and C_i are the resistance and capacitance of the ith RC branch, V_L is the load voltage across the cell terminals, and I_{cell} is the current through the cell (considered positive in discharge and negative in charge). Previous literature has concluded that all these parameters are dependent on SOC, current direction, and temperature of the battery. The circuit output equation of the second order model is given by:

$$V_L = \left(V_{OC} - \sum_{i=1}^{2} V_{Ci} - V_h\right) - I_{cell} \cdot R_0 \tag{12}$$

Each RC circuit is described by an ordinary differential equation obtained using Kirchoff's current law:

$$\frac{dV_{Ci}}{dt} = -\frac{V_i}{V_{Ci}R_i} + \frac{1}{C_i} \cdot I_{cell} \tag{13}$$

The SOC of the battery cell is the ratio of the amount of charge left in a cell and the total charge cell capacity, Q_{cell}. Through current integration, the SOC at each time can be calculated as:

$$SOC(t) = SOC(0) - \frac{\int_0^t I_{cell}(t)dt}{Q_{cell}} \tag{14}$$

The dynamics of the SOC can then be expressed as:

$$\dot{SOC} = -\frac{I_{cell}}{Q_{cell}} \tag{15}$$

Because the parameters of the battery circuit are a function of the SOC, current direction, and temperature, Eq. (15) is a non-linear equation. The parameters of a specific battery can be experimentally determined as shown by Hu et al. [37]. The process involves a multi-layer least square minimization to obtain all of the parameters of the equivalent circuit model. A specifically designed set of

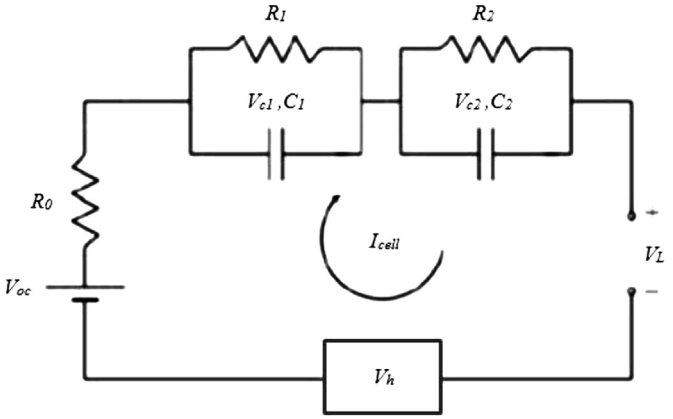

Fig. 6. Battery 2nd order equivalent electrical circuit model.

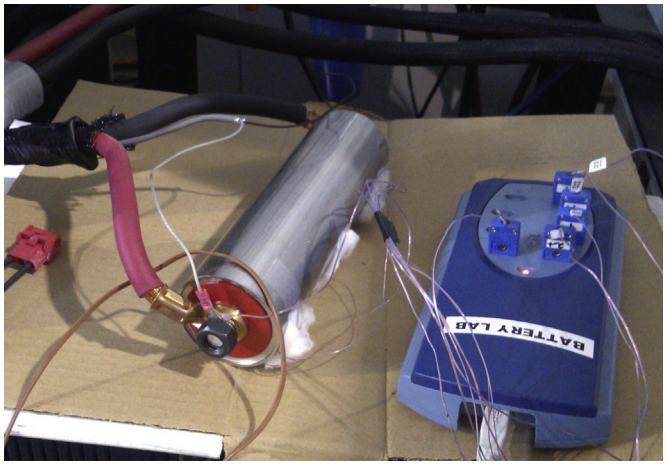

Fig. 7. GAIA LFP battery cell.

experiments spanning the entire range of desired validity of the model in SOC and current dynamics were conducted to validate the battery model in Fig. 6. Typically, the model is validated at several fixed temperatures as well and spliced together using linear splines. However, for this study, proper heat removal from the pack was assumed, limiting temperature variation in the cells, therefore eliminating the parameters' dependence on temperature.

For the battery selected in this study (GAIA LFP), shown in Fig. 7, the parameters of the second order model were identified experimentally at the CAR at OSU. To obtain the most accurate model representation of the battery for its intended operation on the bus, the identification process was completed for an SOC range of [30–80]%, representing the allowable SOC range of the battery for normal operation in the vehicle. A temperature of 25 °C was used for identification. Fig. 8 shows validation of the model by comparing the predicted battery behavior by the model to the experimental data, with a root-mean-square error of 13 [mV].

Over the selected SOC range, it was found that C_1, R_1, C_2, R_2, V_h, and R_0 are only dependent on current direction. The V_{OC} on the other hand is only dependent on SOC. The identified parameters are shown in Table 4. Fig. 9 shows the battery V_{OC} over the entire SOC range.

The battery pack implemented on the bus consists of 180 cells in series, S, and 2 strings of cells in parallel, P, to achieve an nominal 45 kWh energy capacity. The current (I_{batt}) and voltage (V_{batt}) at the pack level can be calculated by:

$$I_{batt} = I_{cell} \cdot P \tag{16}$$

Table 4
LFP battery model parameters over SOC = 30–80%.

Parameter	Charge	Discharge
R_0 [Ω]	$1.0e^{-4}$	$8.0e^{-5}$
C_1 [F]	$2.0e^{4}$	$2.0e^{4}$
R_1 [Ω]	$7.8e^{-4}$	$8.0e^{-4}$
C_2 [F]	$2.0e^{5}$	$2.2e^{5}$
R_2 [Ω]	$3.0e^{-3}$	$3.0e^{-4}$
V_h [V]	$-2.0e^{-3}$	$1.0e^{-3}$

$$V_{batt} = V_L \cdot S \tag{17}$$

3.2.5. Electric motor

The two EMs on the bus convert the electrical power supplied by the fuel cell and battery into a rotational mechanical power. This conversion involves an efficiency loss, η_{EM}. The motors are modeled as static models which use an experimentally obtained efficiency map for calculations, shown in Fig. 10.

3.2.6. Auxiliary loads

The auxiliary loads for a passenger bus can be much greater than those of a light duty passenger vehicle. The power required for heating and cooling, the numerous electronics, automatic doors, etc. can be a significant portion of the overall power demand for the bus. For this reason, taking these auxiliary loads into account for the purpose of energy analysis is important. While these auxiliary loads vary with time, a constant auxiliary power demand of $P_{aux,elec} = 10$ kW is used in the simulator to represent the average power demand from all auxiliary loads (excluding the fuel cell compressor).

4. Optimal supervisory energy management: PMP

The objective of an energy management system in a hybrid vehicle is to satisfy the driver's power demand at the wheel while minimizing a certain cost. This cost can be fuel consumed, emissions of greenhouse gases, aging of components, or any combination of these. For this work, only the fuel consumption was considered. In the hybrid fuel cell bus, the optimal controller finds the optimal trajectories for the fuel cell system and battery which will:

- lead to the minimum fuel consumption over a drive cycle.
- maintain physical limitation of the fuel cell, battery, and electric motors.
- maintain SOC within desired region at all times.
- ensure charge sustaining behavior of the battery (beginning and ending SOC are equal).

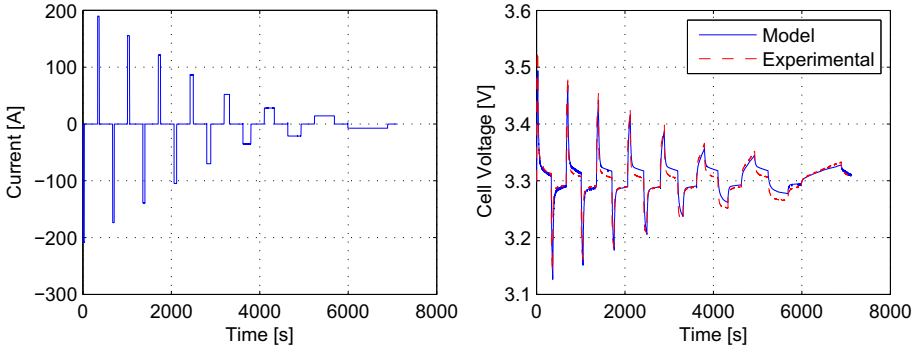

Fig. 8. Battery model validation: input current profile (left) and measured and predicted voltage (right).

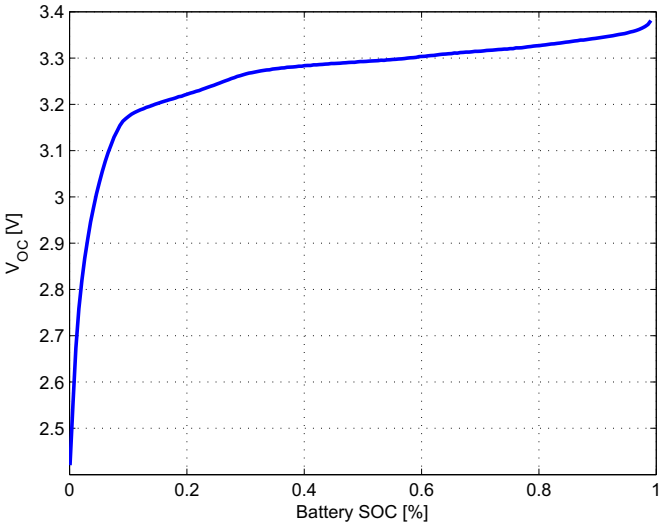

Fig. 9. V_{OC} vs. SOC curve for LFP battery cell.

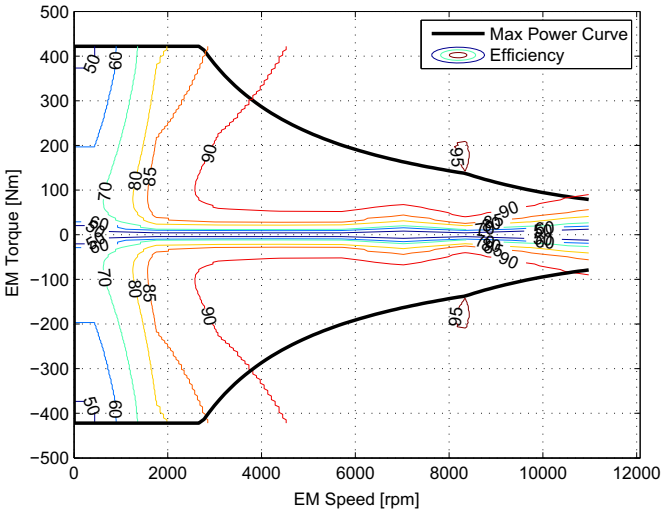

Fig. 10. Electric motor efficiency map and power limitations.

Formally, the energy management of the bus can be formulated as a constrained optimization problem where the mass of hydrogen consumed, m_H, is minimized over a given drive cycle. Since we are interested in monitoring SOC fluctuations over the duration of the drive cycle, the SOC dynamics are modeled and taken as the dynamic state to be optimally controlled. The optimization problem consists of minimizing J:

$$J = \int_0^{t_f} \dot{m}_H(t, P_{batt}(t))dt \tag{18}$$

subject to the following dynamic and static constraints:

$$\dot{SOC}(t) = -\frac{I_{batt}(t)}{Q_{batt}} \tag{19}$$

$$SOC_{min} \le SOC(t) \le SOC_{max} \tag{20}$$

$$SOC(0) = SOC\left(t_f\right) = SOC_{ref} \tag{21}$$

$$P_{batt,min}(t) \le P_{batt}(t) \le P_{batt,max}(t) \tag{22}$$

$$0 \le P_{FC}(t) \le P_{FC,max} \tag{23}$$

$$P_{EM,min}(\omega(t)) \le P_{EM}(t) \le P_{EM,max}(\omega(t)) \tag{24}$$

where SOC_{ref} is the reference SOC, which is known and taken to be 60% in this work. SOC_{min} and SOC_{max} are the minimum and maximum allowable SOC of the battery which are 30% and 80% respectively, for this work, and t_f is the total duration of the drive cycle. The physical limitations of the fuel cell system and electric motors are incorporated through Eqs. (23) and (24). $P_{FC,max}$ is the maximum possible power output of the fuel cell stack, and $P_{EM,min}$ and $P_{EM,max}$ are the minimum and maximum possible EM output power values at a given EM speed (proportional to vehicle speed), ω.

PMP has been applied to the energy management control problem of both a charge sustaining hybrid electric vehicle and to a fuel cell vehicle [24,38] as a proxy for global optimality. In this work, PMP is being used as a means to extract information from the optimal solutions in order to design a practical controller. Moreover, the PMP solutions will serve as a benchmark for comparison, which will aid in calibration of the practical controller. To express the system dynamics, Eq. (19), as a function of the control parameter, P_{batt}, the battery current, I_{batt}, is calculated to be a function of P_{batt}. From the equivalent electric circuit of the battery, described in Section 3.2, the battery power is given by:

$$P_{batt} = V_{batt} \cdot I_{batt} = \left(V_{OC} - \sum_{i=1}^{2} V_{Ci} - V_h\right) \cdot I_{batt} - I_{batt}^2 \cdot R_0 \tag{25}$$

Because V_{Ci}, is dependent on the history of $I_{batt}(t)$, and V_h and R_0 are dependent on the directionality of $I_{batt}(t)$, an explicit solution for I_{batt} cannot be found from Eq. (25). However $I_{batt}(t)$ is calculated in simulation using its discrete time approximation, $I_{batt,k}$, using the previous time-step values of $V_{Ci,k-1}$, $V_{h,k-1}$, and $R_{0,k-1}$:

$$I_{batt,k} = \frac{\left(V_{OC,k} - \sum_{i=1}^{2} V_{Ci,k-1} - V_{h,k-1}\right) - \sqrt{\left(V_{OC,k} - \sum_{i=1}^{2} V_{Ci,k-1} - V_{h,k-1}\right)^2 - 4 \cdot R_{0,k-1} \cdot P_{batt,k}}}{2 \cdot R_{0,k-1}} \tag{26}$$

where k is the discrete sampling time. With I_{batt} given in Eq. (4), the SOC dynamics in Eq. (19) can be expressed as a function of P_{batt}. PMP introduces the Hamiltonian function [23], given by:

$$H = \lambda(t) \cdot \dot{SOC}(SOC(t), P_{batt}(t), t) + \dot{m}_H(P_{batt}(t), t) \tag{27}$$

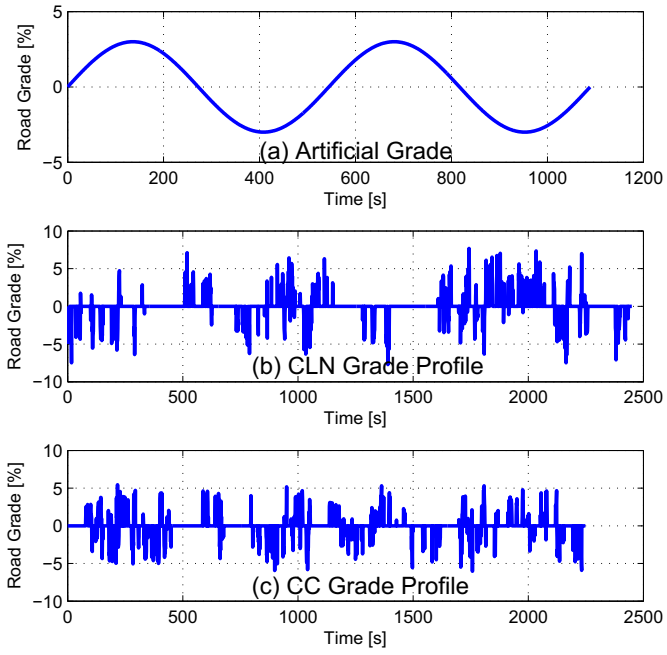

Fig. 11. Drive cycle grade profiles.

where $\lambda(t)$ is the co-state variable which varies with time and is unknown. PMP provides a set of necessary conditions that must be satisfied by the optimal control trajectory, $P^*_{\text{Batt}}(t)$. Applied to the fuel cell hybrid bus energy management control problem, they are:

$$\dot{\lambda}^*(t) = -\frac{\partial H\left(\text{SOC}^*(t), P^*_{\text{Batt}}(t), \lambda^*(t), t\right)}{\partial \text{SOC}} \tag{28}$$

$$\dot{\text{SOC}}^*(t) = \frac{\partial H\left(\text{SOC}^*(t), P^*_{\text{Batt}}(t), \lambda^*(t), t\right)}{\partial \lambda} \tag{29}$$

$$\text{SOC}^*(0) = \text{SOC}_{\text{ref}} \tag{30}$$

$$\text{SOC}^*\left(t_f\right) = \text{SOC}_{\text{ref}} \tag{31}$$

$$\text{SOC}_{\text{min}} \le \text{SOC}^*(t) \le \text{SOC}_{\text{max}} \tag{32}$$

where * denotes the optimal value of the variable. PMP states that the optimal trajectories minimize the Hamiltonian such that:

$$H\left(\text{SOC}^*(t), P^*_{\text{Batt}}(t), \lambda^*(t), t\right) \le H\left(\text{SOC}^*(t), P_{\text{Batt}}(t), \lambda^*(t), t\right) \tag{33}$$

The Hamiltonian can be minimized at each instant in time which will lead to the optimal control trajectory. The dynamic equations in Eqs. (28) and (29) are dependent on their initial conditions. The initial SOC of the battery is known *a priori* as well as the final SOC (charge sustainability). However, the initial condition of the co-state, λ_0 is unknown. It turns out that λ_0 is the principal parameter of the PMP optimal controller. The value of λ_0 can be tuned through the shooting method [30] which consists of guessing values of λ_0, running simulations, and selecting the one which satisfies Eq. (31). Finding the optimal solution reduces to finding the λ^*_0, which is unique for each drive cycle.

Once λ^*_0 is found, the PMP controller provides the SOC and control trajectories for a given drive cycle which minimize the hydrogen fuel consumption of the fuel cell.

Table 5
Statistics of drive cycles.

Name	V_{rms} [m s^{-1}]	V_{mean} [m s^{-1}]	V_{max} [m s^{-1}]	a_{rms} [m s^{-2}]
MAN	3.0	4.5	11.2	0.6
HDUDDS	8.4	12.2	25.9	0.4
CLN	4.0	5.7	17.7	0.6
CC	4.3	6.2	17.9	0.6

Table 6
PMP results.

Cycle	λ_0 [kg]	Average fuel cell power output [kW]	Fuel economy [mpg diesel equivalent]
MAN	1,992,220	29.6	5.64
MAN w/grade	1,999,720	31.4	5.30
HDUDDS	2,070,610	46.5	9.77
HDUDDS w/grade	2,081,025	49.6	9.13
CLN w/grade	2,014,460	34.2	6.40
CC w/grade	2,015,215	35.0	6.69

5. PMP simulation results

The optimal PMP controller was implemented in the fuel cell bus simulator under the following scenarios:

- Manhattan driving cycle (MAN)
- Heavy Duty Urban Dynamometer Driving Schedule (HDUDDS)
- OSU Campus Area Bus Service real world drive cycles,
- Campus Loop North (CLN)
- Central Connector (CC)

The MAN and HDUDDS drive cycles are standard cycles which do not contain a corresponding road grade profile. To test the effects that the road grade would have on the controller results, these cycles were simulated with and without an artificial, sinusoidal road grade with a maximum amplitude of ±3% as shown in Fig. 11(a). The CLN and CC drive cycles were experimentally obtained from actual bus routes on the OSU campus, and have corresponding road grade profiles, shown in Fig. 11(b) and (c). Table 5 provides metrics for each drive cycle examined such as the RMS velocity,[2] V_{rms}, mean velocity, V_{mean}, max velocity, V_{max}, and the RMS acceleration,[2] a_{rms}.

The simulation results are summarized in Table 6. The equivalent fuel economy is calculated by:

$$\begin{aligned} \text{gallon diesel equiv} &= \frac{M_{\text{H}} \cdot \text{LHV}_{\text{H}}}{\rho_{\text{d}} \cdot \text{LHV}_{\text{d}}} \cdot 0.2642 \\ \text{mpg diesel equiv} &= \frac{\text{miles traveled}}{\text{gallon diesel equiv}} \end{aligned} \tag{34}$$

where M_{H} [kg] is the equivalent mass of hydrogen consumed, LHV_{H} and LHV_{d} [kJ kg^{-1}] are the lower heating values of hydrogen and Diesel fuel respectively, ρ_{d} [kg l^{-1}] is the density of Diesel fuel, and 0.2642 is the conversion from l to gallons.

A comparison of the results and trajectories for the MAN, HDUDDS, drive cycles without grade, and CLN drive cycle with grade are shown in Fig. 12.

[2] For a given vector X, the RMS value is defined as: $X_{\text{rms}} = \sqrt{\sum_{i=1}^{n} X_i^2 / n}$ where n is the length of the vector.

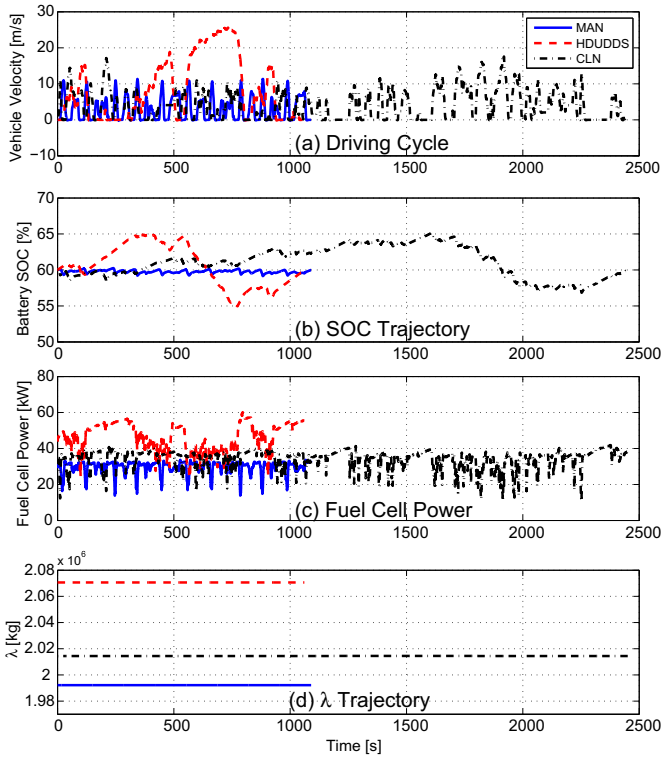

Fig. 12. Simulation results using PMP optimal controller for different drive cycles of different duration: Manhattan without grade, HDUDDS without grade, and CLN with grade. (a) Shows the velocity profile for each cycle, (b) provides the SOC trajectory of the battery, (c) shows the fuel cell power demand, and (d) shows the λ trajectory for each case.

By observing Fig. 12(d) it can be seen that for different drive cycles, the value of λ is different. However, in spite of Eq. (28), λ is essentially constant for the duration of the trip. The severity of the HDUDDS cycle, which consists of large accelerations with relatively high speeds, is much larger than the other two cycles depicted. This leads to a much large value of λ.

From Fig. 12(c) we can see that a higher λ value leads to an overall higher power demand from the fuel cell. While there are fluctuations in fuel cell operation in every case, the fuel cell operates mainly around a centralized (average) value for each cycle.

For the MAN cycle, which consists of multiple stops and has the lowest average and maximum velocities among the cycles examined, the range of SOC explored is very small, seen in Fig. 12(b). However, for the HDUDDS cycle a larger range of SOC is explored, with a large drop in SOC occurring during an acceleration to high speed (around $t = 600$ s), seen in Fig. 12(a). Similarly, for the CLN cycle the SOC gradually increases until multiple high speed accelerations occur (around $t = 1600$ s). At this point, the battery is used to meet the large power demands, decreasing the SOC. By design, charge sustainability is achieved for each drive cycle.

Table 7
ARMA parameters.

Parameter	Value
j	10 s
N	25
M	1
α_i	Description to follow
β_i	$\beta_1 = 16$
$P_{FC}(0)$	Description to follow

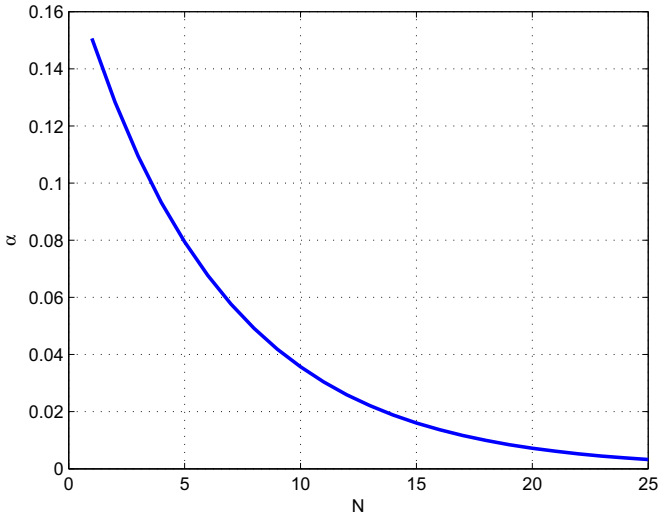

Fig. 13. Values of α with respect to N used to calibrate the AR portion of the practical controller.

6. Practical controller implementation

The optimal PMP controller is difficult to implement in real time. As shown previously, the optimal solution can only be achieved when the proper value of λ_0 is selected. However, because this value depends on the drive cycle, optimality and charge sustainability can not be guaranteed for real time implementation, when the drive cycle is not known *a priori*. Because of this, design of a rule-based or simple algorithmic controller for implementation on the hybrid fuel cell bus is needed. The controller should mimic the tendencies of the PMP controller in order to be as close to optimal as possible. The optimal PMP results show the following:

- λ is nearly constant during a given drive cycle;
- the optimal λ_0 is dependent on the severity of the drive cycle;
- fuel cell shows a relatively narrow range of operation around the average power demand for a given drive cycle;
- average fuel cell power demand is related to the severity of the drive cycle.

Based on these results, the following ARMA controller is proposed:

$$P_{FC}(j+1) = \sum_{i=1}^{N} \alpha_i \cdot P_{FC}(j+1-i) + \sum_{j=1}^{M} \beta_j \cdot \left(\mathrm{SOC}(j+1-j) - \mathrm{SOC}_{\mathrm{ref}}(j)\right) \tag{35}$$

where the first term is the auto-regressive weighted average of N past values of P_{FC} and the second term is the weighted average of M

Table 8
ARMA results.

Cycle	Average fuel cell power output [kW]	Fuel economy [mpg diesel equivalent]	% Difference from PMP results [%]
MAN	29.8	5.63	−0.2
MAN w/grade	32.7	5.15	−2.8
HDUDDS	44.9	9.55	−2.3
HDUDDS w/grade	49.1	9.04	−1.0
CLN w/grade	31.7	6.35	−0.8
CC w/grade	35.9	6.56	−1.9

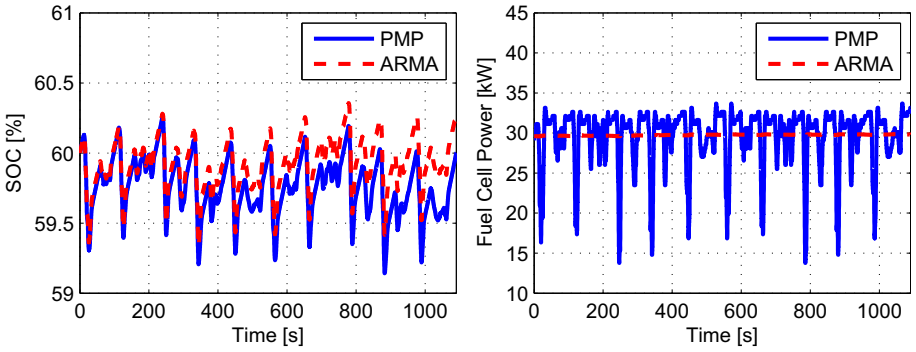

Fig. 14. SOC and P_{FC} trajectories for the Manhattan drive cycle without grade.

past values of the SOC deviation from the target SOC. For stability, $\sum_{i=1}^{N}\alpha_i = 1$, and β_j can be interpreted as the gains of an extended PI controller. j is an index of adaptation time, where the period of adaptation can be tuned for a desired performance.

This control strategy is inherently low pass filtering, hence limiting the fuel cell transients, which will prolong the life of the fuel cell. Initial examination of the algorithm also indicates that it is inherently smoothing, immune to noise, and capable of adapting to changes in the severity of the driving conditions. It also operates the fuel cell in a manner similar to what was seen by the PMP controller, and results in an SOC trajectory similar to the PMP controller. The calibration of the practical controller defined in Eq. (35) should guarantee sub-optimal performance over a wide range of operation of the bus. Therefore, the controller parameters have been tuned to achieve performance to mimic behaviors seen from the PMP controller. If was found that the performance of the controller with respect to fuel consumption was relatively insensitive to changes of these parameter values. The optimal parameter values of the ARMA controller found from this analysis are presented below in Table 7.

The values of α were found using a decreasing exponential function, shown in Eq. (36), to allow more recent fuel cell set points to have the largest impact. The values of α can be seen in Fig. 13.

$$\alpha_i = \exp\left(-\frac{N-i+1}{4\cdot N}\right) = \frac{\alpha_i}{\sum_{i=1}^{N}\alpha_i} \tag{36}$$

The initial fuel cell set point is needed in order to simulate the ARMA controller. This value was set for each drive cycle as the average fuel cell power demand obtained from the PMP controller. These values can be found in Table 6. For application on the actual bus, this value could be calculated from the previous day of operation, since the bus would be expected to see very similar duty cycles from day to day.

The same drive cycles were simulated using the ARMA controller for comparison with the PMP results. Because the ARMA controller does not guarantee the ending SOC is equal to the initial SOC, that change in energy must be taken into account when calculating fuel economy:

$$M_{eq} = \int_0^{t_f} \dot{m}_H + \frac{\int_0^{t_f} P_{batt}}{LHV_H \cdot \eta_{path}^{sign(\Delta SOC)}} \tag{37}$$

where M_{eq} is the equivalent mass of hydrogen consumed, and η_{path} is the average powertrain efficiency which was estimated to be 40%. ΔSOC is:

$$\Delta SOC = SOC\left(t_f\right) - SOC(0) \tag{38}$$

Eq. (34) still applies, where M_{eq} can be used in place of M_H. The ARMA controller was capable of achieving fuel economy of 5.1–9.5 mpg diesel equivalent, depending on drive cycle. The results are summarized in Table 8

Results also show that the controller minimizes transients on the fuel cell system. This will lead to prolonged life of the fuel cell. While the fuel cell operation is somewhat different between the PMP and ARMA controllers, the resulting SOC trajectory of the battery are very similar, as shown in Figs. 14–16 for the MAN, HDUDDS, and CLN drive cycles respectively.

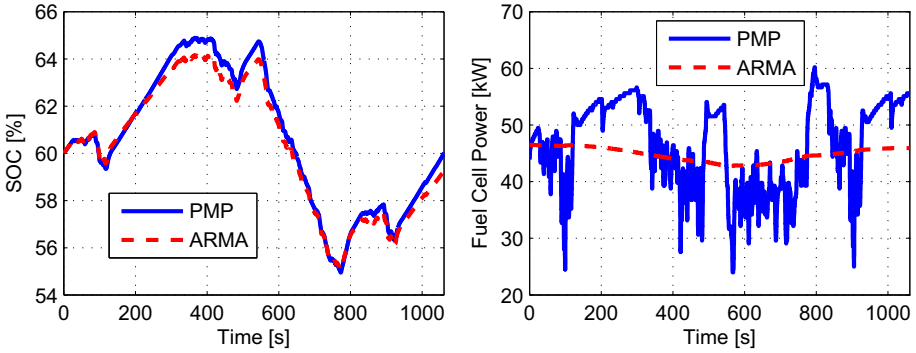

Fig. 15. SOC and P_{FC} trajectories for the HDUDDS without grade.

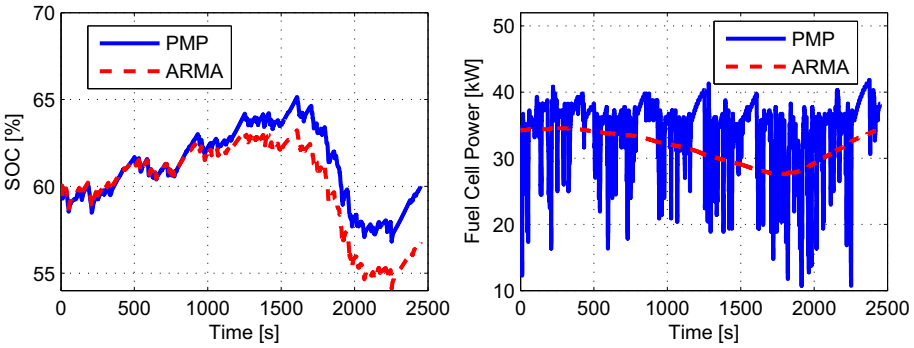

Fig. 16. SOC and P_{FC} trajectories for the CLN drive cycle with grade profile seen in Fig. 11(b).

7. Conclusions

In this paper the modeling of an appropriate energy-based vehicle simulator for a proposed Fuel Cell Hybrid Bus powertrain was presented. The representative simulator was designed for the purpose of energy analysis and control strategy development. The formulation of the optimal energy management problem in the bus was defined. The design approach taken by the authors to develop a real-time controller for the bus was to first find the optimal solutions for multiple drive cycles, with and without grade, using PMP, and then develop an implementable controller based on observations and analysis of the optimal solutions.

An analysis of the optimal control obtained from the PMP controller showed that the initial value of the co-state which leads to the optimal trajectory was dependent on the severity of the given drive cycle. Also, the variation of λ with respect to time is negligible for the duration of a driving event. The results also show that the optimal fuel cell operation is dependent on the severity of the drive cycle.

These observations led to the design of a practical controller in the form of an ARMA regulator. Results from simulations using the ARMA controller were presented and compared to the optimal case. The ARMA controller performed well, achieving sub-optimal fuel economy values that were less than a 3% decrease from the optimal value for each drive cycle tested. It was found that overall fuel consumption was insensitive to changes in the parameters of the controller. Also, the controller allowed for limited transients on the fuel cell system, so prolonging the life of the system. The ARMA controller is well suited for on-board implementation as it requires minimal computational effort with low memory requirements, and in the future, it will be implemented on the actual bus.

References

[1] A. Bredenberg, The damage done in transportation – which energy source will lead to the greenest highways?, IMT Green Clean Journal RSS.
[2] D. Crolla, Q. Ren, S. ElDemerdash, F. Yu, Controller design for hybrid vehicles – state of the art review, in: Vehicle Power and Propulsion Conference, 2008, pp. 1–6.
[3] L. Xu, J. Li, J. Hua, X. Li, M. Ouyang, Journal of Power Sources 194 (1) (2009) 360–368.
[4] L. Eudy, K. Chandler, C. Gikakis, Fuel Cell Busses in U.S. Transit Fleets: Current Status 2012. Tech. rep., National Renewable Energy Laboratory, 2012
[5] [link], URL: http://www.designlinecorporation.com/.
[6] L.S. Pontryagin, V.G. Boltyanski, R.V. Gamkrelidze, E.F. Mischenko, The Mathmatical Theory of Optimal Processes, CRC Press, 1962.
[7] A. Sciarretta, L. Guzzella, IEEE 27 (2) (2007) 60–70.
[8] G. Paganelli, Y.M. Guerra, S. Delprat, Y. Guezennec, G. Rizzoni, Optimal Control Theory Applied to Hybrid Fuel Cell Powered Vehicle, July 2002.
[9] G. Paganelli, Y. Guezennec, G. Rizzoni, Optimizing control strategy for hybrid fuel cell vehicle.
[10] Y. Guezennec, T.-Y. Choi, G. Paganelli, G. Rizzoni, Supervisory control of fuel cell vehicles and its link to overall system efficiency and low-level control requirements, in: American Control Conference, Proceedings of the 2003, vol. 3, 2003, pp. 2055–2061.
[11] T. Hofman, M. Steinbuch, R. Druten, A. Serrarens, International Journal of Electric and Hybrid Vehicles 1 (8) (2007) 7–94.
[12] B. Baumann, G. Washington, B. Glenn, G. Rizzoni, Mechatronic design and control of hybrid electric vehicles, IEEE/ASME Transactions on Mechatronics 5 (1) (2000) 58–72.
[13] J.-S. Won, R. Langari, Expert Systems 19 (1) (2002) 4–10.
[14] T. Hofman, M. Steinbuch, R. van Druten, A. Serrarens, in: Proceedings of the 17th IFAC World Congress, 2008.
[15] C. Musardo, G. Rizzoni, B. Staccia, A-ECMS: an adaptive algorithm for hybrid electric vehicle energy management, in: IEEE Conference on Decision and Control, 2005, pp. 1816–1823.
[16] C.-Y. Li, G.-P. Liu, Journal of Power Sources 192 (2) (2009) 525–533.
[17] X. Li, L. Xu, J. Hua, X. Lin, J. Li, M. Ouyang, Journal of Power Sources 191 (2) (2009) 542–549.
[18] G. Paganelli, S. Delprat, T.-M. Guerra, J. Rimaux, J.J. Santin, Equivalent consumption minimization strategy for parallel hybrid powertrains, in: Vehicular Technology Conference, vol. 4, 2002, pp. 2076–2081.
[19] G. Paganelli, T. Guerra, S. Delprat, J. Santin, M. Delhom, E. Combes, Journal of Automobile Engineering 214 (7) (2000) 705–717.
[20] P. Rodatz, G. Paganelli, A. Sciarretta, L. Guzzella, Control Engineering Practice 13 (1) (2005) 41–53.
[21] G. Paganelli, G. Ercole, A. Brahma, Y. Guezennec, G. Rizzoni, JSAE Review 22 (4) (2001) 511–518.
[22] C. Musardo, B. Staccia, S. Midlam-Mohler, Y. Guezennec, G. Rizzoni, Supervisory control for NOx reduction of an HEV with a mixed-mode HCCI/CIDI engine, in: American Control Conference, vol. 6, 2005.
[23] H.P. Geering, Optimal Control with Engineering Applications, Springer, 2007.
[24] J. Bernard, S. Delprat, T. Guerra, F. Bchi, Control Engineering Practice 18 (4) (2010) 408–417.
[25] D. Feroldi, M. Serra, J. Riera, Journal of Power Sources 190 (2) (2009) 387–401.
[26] S. Delprat, J. Lauber, T.-M. Guerra, J. Rimaux, IEEE Transactions on Vehicular Technology 53 (3) (2004) 872–881.
[27] J. Bernard, S. Delprat, F. Buechi, T. Guerra, Global optimisation in the power management of a fuel cell hybrid vehicle (FCHV), in: Vehicle Power and Propulsion Conference, 2006, IEEE, 2006, pp. 1–6.
[28] A. Brahma, Y. Guezennec, G. Rizzoni, Optimal energy management in series hybrid electric vehicles, in: American Control Conference, vol. 1, 2000, pp. 60–64.
[29] L. Xu, M. Ouyang, J. Li, F. Yang, Dynamic programming algorithm for minimizing operating cost of a PEM fuel cell vehicle, in: IEEE International Symposium on Industrial Electronics (ISIE), 2012, pp. 1490–1495.
[30] L. Serrao, S. Onori, G. Rizzoni, ASME Journal of Dynamic Systems, Measurement and Control 133 (2011) 1–9.
[31] C.-C. Lin, H. Peng, J. Grizzle, J.-M. Kang, IEEE Transactions on Control Systems Technology 11 (6) (2003) 839–849.
[32] D. Gao, C. Mi, A. Emadi, Proceedings of the IEEE 95 (4) (2007) 729–745.
[33] Ballard Power Systems Inc., FCvelocity-HD6 Spec Sheet, URL: http://www.ballard.com/files/PDF/Bus/HD6.pdf.
[34] P.M. Gomadam, J.W. Weidner, R.A. Dougal, R.E. White, Journal of Power Sources 110 (2) (2002) 267–284.
[35] A. Ledovskikh, E. Verbitskiy, A. Ayeb, P. Notten, Journal of Alloys and Compounds 356–357 (2003) 742–745.
[36] Y. Hu, S. Yurkovich, Y. Guezennec, B. Yurkovich, Control Engineering Practice 17 (10) (2009) 1190–1201.
[37] Y. Hu, S. Yurkovich, Y. Guezennec, B. Yurkovich, Journal of Power Sources 196 (1) (2011) 449–457.
[38] L. Serrao, S. Onori, G. Rizzoni, ECMS as a realization of Pontryagin's Minimum Principle for HEV control, in: American Control Conference, 2009, pp. 3964–3969.